Device modelling of non-fullerene organic solar cell with inorganic CuI hole transport layer using SCAPS 1-D

2 authors:

Nithya K S
Christ College, Irinjalakuda
4 PUBLICATIONS   **5** CITATIONS

SEE PROFILE

Sudheer Sebastian
Christ College, Irinjalakuda
13 PUBLICATIONS   **325** CITATIONS

SEE PROFILE

Contents lists available at ScienceDirect

Optik

Original research article

Device modelling of non-fullerene organic solar cell with inorganic CuI hole transport layer using SCAPS 1-D

K.S. Nithya*, K.S. Sudheer

Opto-electronic device simulation research lab, Department of Physics, Christ College(Autonomous)Irinjalakuda, University of Calicut, Kerala, India

A R T I C L E   I N F O

A B S T R A C T

Hole transport layer (HTL) plays a significant role in the device performance of organic solar cells. PEDOT:PSS, the most commonly used HTL degrades the device and effects the stability of Organic solar cell (OSC). An alternate material to maximise the output of OSC is necessary. In this paper, a complete simulation study on the performance of (PBDB-T) poly[(2,6-(4,8-bis(5-(2-ethylhexyl)thiophen-2-yl)benzo[1,2-b:4,5-b]dithiophene)-co-(1,3-di(5-thiophene-2-yl)-5,7-bis(2-ethylhexyl)benzo[1,2-c:4,5-c]dithiophene-4,8-dione)/(ITIC)3,9-bis(2-methylene-(3-(1,1-dicya-nomethylene)-indanone)-5,5,11,11-tetraki(4-hexylphenyl)-dithieno[2,3-d:2,3-d]-s-indaceno [1,2-b:5,6-b]dithiophene) non-fullerene acceptor (NFA) OSC incorporated with Copper iodide (CuI) as HTL is done using the software SCAPS 1-D. Device modelling is done to study the influence of various technological parameters on the solar cell output. CuI is wider bandgap p-type semiconductor with high stability and available at low cost. The simulation results show that NFA-OSC with CuI as the HTL delivers better efficiency than the conventional structure. Upon optimization, the device output shows Power conversion efficiency (PCE) of 15.68%, Fill Factor (FF) of 79.59%, Short Circuit Current density (Jsc) of 20.1525 mA/$^{cm^2}$ and Open Circuit Voltage (Voc) of 0.9773 V. The values are encouraging to develop NFA-OSC with CuI as the hole transport layer in the near future.

1. Introduction

Organic photovoltaics has been showing significant improvement in the recent years [1–4]. Non-fullerene acceptors (NFA) overcome the morphological instabilities of their fullerene counterparts and appears to be one of the suitable candidate for developing high efficiency organic solar cell (OSC) [5–13]. Having a hole transport layer (HTL) between the polymer and electrode tunes the work function of electrodes along with reducing the undesired quenching of excitons at the electrode surfaces and also reduces the carrier recombination [14–17]. The most commonly used HTL in conventional OSC is PEDOT:PSS thanks to its high conductivity, high work function and improved transparency [18,19]. However, PEDOT:PSS degrades the device due to its acidic and hygroscopic nature and its capability to block electron is uncertain owing to its use as electron collecting electrode [20–23]. It is extremely sufficient for OSC devices to improve charge transport towards the respective electrodes for reducing the charge recombination and to ensure that, a lot of alternate HTL materials have been studied [24–30].

Copper iodide (CuI) with a wider bandgap of 2.98 eV consists of three crystalline phases α, β and γ [31]. Among them, γ phase CuI behaves as a typical p-type semiconductor and has favourable fermi level energy and efficient optical transparency. Zhou et al. reported the use of CuI nanocrystals in ZnPC:C60 bilayer organic solar cell [32] and Shao et al. showed that P3HT:PCBM film

---

* Corresponding author.
E-mail address: nithyaks@christcollegeijk.edu.in (K.S. Nithya).

deposited on CuI has higher mobility than those deposited on PEDOT:PSS [33]. Experimental works on CuI as the hole transport layer for BHJ solar cells shows better performance than the conventional device using PEDOT:PSS [34]. The improvement in device performance was basically owed to achieving a higher fill factor due to reduced series resistance Rs and improved shunt resistance Rsh.

NFA-OSC with CuI as the hole transport layer provides a better alternative for photovoltaics. ITIC (3,9-bis(2-methylene-(3-(1,1-dicyanomethylene)-indanone)-5,5,11,11-tetraki (4-hexylphenyl)-dithieno[2,3-d:2,3-d]-s-indaceno[1,2-b:5,6-b]dithiophene)) is one of the most effective NFA, first introduced by Zhane et al. [35]. PBDB-T(poly[(2,6-(4,8-bis(5-(2-ethylhexyl)thiophen-2-yl) benzo[1,2-b:4,5-b]dithiophene)-co-(1,3-di(5-thiophene-2-yl)-5,7-bis(2-ethylhexyl)benzo[1,2-c:4,5-c]dithiophene-4,8-dione)]) enhances the absorption spectrum and the BHJ combination of PBDB-T/ITIC has been showing a lot of potential in recent years [36–41]. Device modelling of PBDB-T/ITIC solar cell with PEDOT:PSS as HTL is already reported in the literature [43]. No computational studies have been done so far to explore the incorporation of CuI to the NFA-OSC and device modelling is an efficient tool to understand and optimize the device parameters to design highly efficient OSC for future.

In this work, One dimensional Solar Cell Capacitance Simulator (SCAPS) is used to numerically simulate PBDB-T/ITIC blend with CuI as the HTL and PFN-Br as the electron transport layer (ETL) [59]. SCAPS has been used extensively to simulate various types of solar cells including NFA-BHJ [42–51]. Software is calibrated using control variable method and a comprehensive device modelling is done for the NFA-Bulk heterojunction to study the influence of material parameters on the output performance of the organic solar cell.

2. Device modelling parameters

Bulk heterojunction structure of NFA-OSC with the layer configuration of glass substrate/ITO/CuI/PBDB-T/ITIC/PFN-Br/Ag is simulated using SCAPS 1-D. The simulated solar cell configuration with PFN-Br as the ETL, CuI as the HTL, PBDB-T/ITIC as the active layer, ITO and Ag as the front and back electrodes respectively is given in Fig. 1(a). The energy band alignment is shown in Fig. 1(b).

The valence band offset at Active/CuI interface is $+0.6$ eV providing an easy pathway for holes to flow to the back metal contact while the conduction band offset at PFN-Br/Active interface is $+0.71$ eV, which is crucial for the migration of generated photoelectrons to the front contact. Table 1 summarises the simulation parameters for the configuration. The given parameters E_g is the energy bandgap, ϵ_r is the relative permittivity, χ being the electron affinity, μ_n and μ_p are the electron and hole mobilities, N_t is the defect density respectively. N_A and N_D are the densities of acceptor and donor materials whereas N_C and N_V are the effective densities of conduction band and valence band [42]. The parameter values not included in the table are set identical for all layers. Neutral gaussian distribution defect is adopted with characteristic energy being set to 0.1 eV. The electron and hole capture cross cross section is set to 9×10^{-15} $^{cm^2}$ with the thermal velocity of both carriers are fixed at 10^7 cm/s [43]. Two defined defect interfaces HTL/Active and Active/ETL is set with a concentration of 10^9 cm^{-2}. Work function of the front electrode is set to 4.7 eV [59] and that of the back electrode is set to 4.1 eV. The absorption profile for active layer and HTL is obtained from the literature [36,51]. No optical reflectance is considered in the simulation and we have optimized the numerical parameters used in the study using control variable method.

After performing simulations in SCAPS using the parameters in Table 1, we obtained the solar cell output parameters: Open circuit
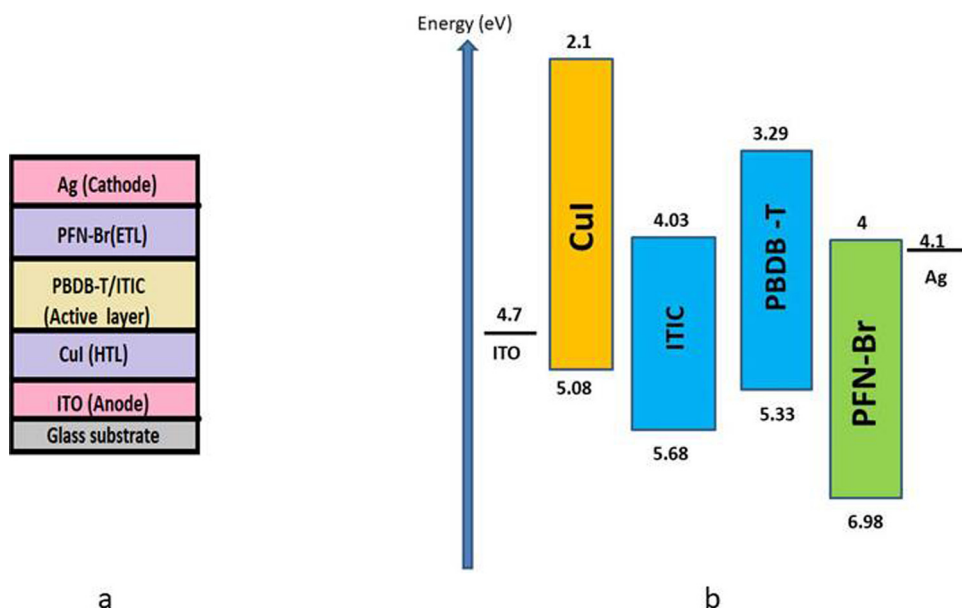

Fig. 1. Simulated solar cell (a) configuration of the cell (b) Enegy band alignment.

Table 1
Numerical parameters used in the simulation.

Parameters	HTL	Active layer	ETL
Thickness (nm)	40	100 [36]	5 [36]
E_g (eV)	2.98 [52]	1.2 [37,43]	2.98 [53]
χ (eV)	2.1 [54]	4.03 [36]	4 [43]
ϵ_r	6.5 [55]	3.65 [36,43]	5 [43]
μ_n (cm^2/vs)	1.69×10^{-4}	3.1×10^{-4} [36]	2×10^{-6} [43]
μ_p (cm^2/vs)	1.69×10^{-4} [56]	3.2×10^{-4} [36]	1×10^{-4} [43]
N_A (cm^{-3})	2×10^{18} [57]	0	0
N_D (cm^{-3})	0	0	9×10^{18}
N_C (cm^{-3})	10^{22} [58]	10^{19} [43]	10^{19} [43]
N_V (cm^{-3})	10^{22} [58]	10^{19} [43]	10^{19} [43]
N_t (cm^{-3})	10^9 [43]	10^{12}	10^9 [43]

voltage (Voc), Short circuit current density (Jsc), Fill factor (FF) and Power conversion efficiency (PCE). The short circuit current density-Voltage (J–V curve) is shown in Fig. 2(a) and the corresponding External quantum efficiency curve (EQE) is shown in Fig. 2(b). The simulated output is consistent with the experimental results for NFA-OSC [36–41]. This shows that the parameters used in the simulation are in close agreement with the real parameters of the device and the software is perfectly calibrated for simulating NFA-OSC. The calibrated cell is simulated to design NFA-OSC with inorganic CuI as the HTL by optimizing the material parameters of the device.

3. Results and discussion

### 3.1. Influence of the thickness of active layer

Thickness of active layer is a crucial parameter in the output performance of solar cell. The active layer thickness is varied in the range from 50 nm to 350 nm and the effect on output is studied as shown in Fig. 3. The Jsc and PCE increases significantly upon increasing the thickness and reaches a maximum value of 20.153 mA/cm^2 and 13.58% at the active layer thickness of 200 nm. This can be due to the improved light absorption and increased photogenerated carriers due to increased thickness. On further increasing the thickness, both PCE and Jsc starts to decrease. Above 200 nm, the carrier diffusion length is more than the active layer thickness and it leads to increase in recombination current and decreased output. Similarly, Voc increases upon improved active layer thickness and beyond the optimum value, it starts to decrease. Voc depends on the dark I–V characteristics of the cell. The small variation in Voc can be attributed to the change in dark saturation current with the variation in active layer thickness. FF is dropping continuously upon increasing the active layer thickness. This can be due to the increase in series resistance of the cell with the improved thickness of active layer.

3.2. Influence of defect density of active layer

The defect density (Nt) has been varied in the range $10^{10\ cm^{-3}}$–$10^{14\ cm^{-3}}$. The effect of defect density is analysed using the Shockley-Read Hall recombination equation [60].

$$R^{SRH} = \frac{np - n_i^2}{\tau_p(n + n_t) + \tau_n(p + p_t)} \tag{1}$$

where n, p refers to the mobile electron-hole concentration, and n_t, p_t being the trap defect concentration with n_i, the intrinsic
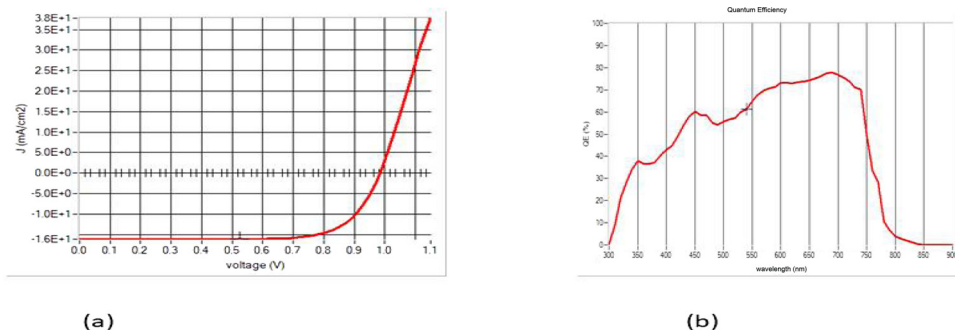
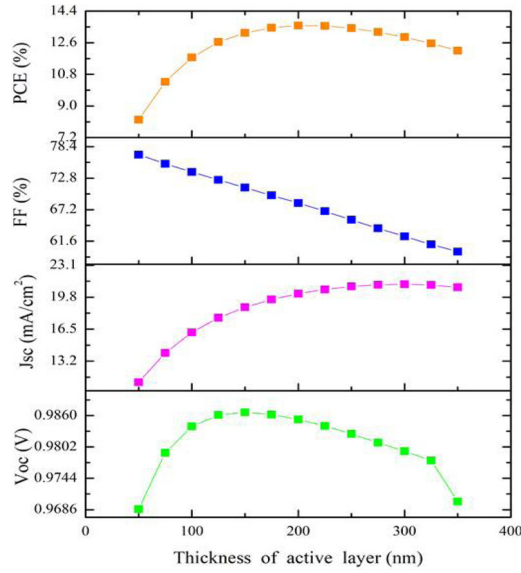**Fig. 2.** Simulated output from SCAPS $(a)J - V$ curve (b) EQE curve.

Fig. 3. Effect of active layer thickness on output parameters.

concentration. The lifetime τ is given by the relation [61]:

$$\tau = \frac{1}{\sigma V_{\text{th}} N_t}$$

(2)

with σ being the capture cross section and N_t, the trap defect density and V_{th} being the carrier thermal velocity. The exciton diffusion length is given by $L = \sqrt{D\tau}$ where D is the diffusion constant.

The output device performance with variation of Nt is given in Fig. 4. As Nt increases, the lifetime of carriers decreases leading to increased recombination rate effecting the output performance. Table 2 shows the variation of electron diffusion length and lifetime upon changing the defect density. The device output is improved upon reducing the defect density below $10^{11}\ cm^{-3}$ with a Jsc of $16.168\ \text{mA}/^{cm^2}$, Voc of 0.9956 V, FF of 76.15% and PCE of 12.26%. But, we cant set the defect density to be $10^{11}\ cm^{-3}$ as it is impossible to realise diffusion length corresponding to this value in organic materials [61]. Thus we have chosen the optimised value to be $10^{12}\ cm^{-3}$.
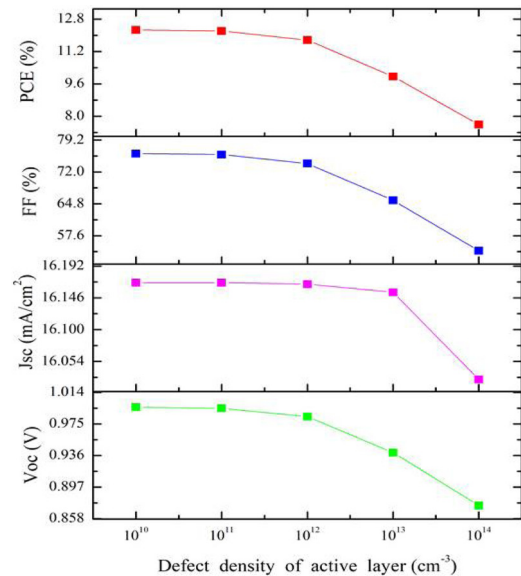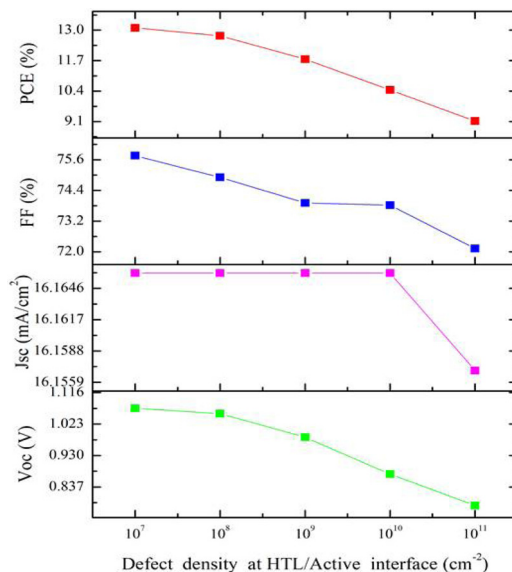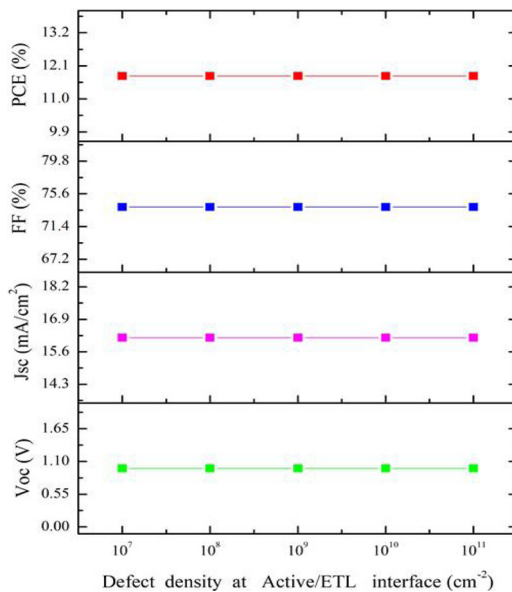

Fig. 4. Effect of defect density of active layer on output parameters.

Table 2
Variation of diffusion length and lifetime of electron with defect density.

N_t (cm^{-3})	10^{10}	10^{11}	10^{12}	10^{13}	10^{14}
L_n (μm)	0.19	0.059	.019	.0059	.0019
τ_n (μs)	1100	110	11	1.1	0.11

Fig. 5. Effect of defect density at HTL/Active interface on output parameters.

Fig. 6. Effect of defect density at Active/ETL interface on output parameters.

3.3. Influence of defect density at interface layers

We have defined two interfaces; HTL/Active and Active/ETL. The simulations are done by varying the defect densitis of both interfaces between the range 10^7 cm^{-2}–10^{11} cm^{-2}. The increase in defect density leads to more traps and degrades the cell output. It is always preferable to have low interface defect densities for better output performance. The effect of variation of defect densities at both interfaces are shown in Figs. 5 and 6 . As it appears from the figure, the Active/ETL interface has no effect on the output
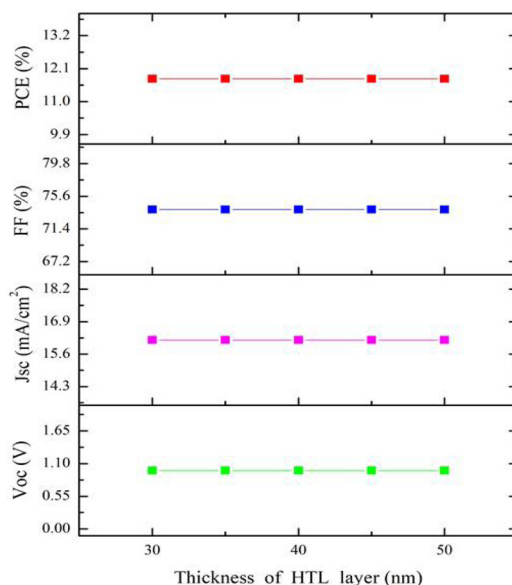
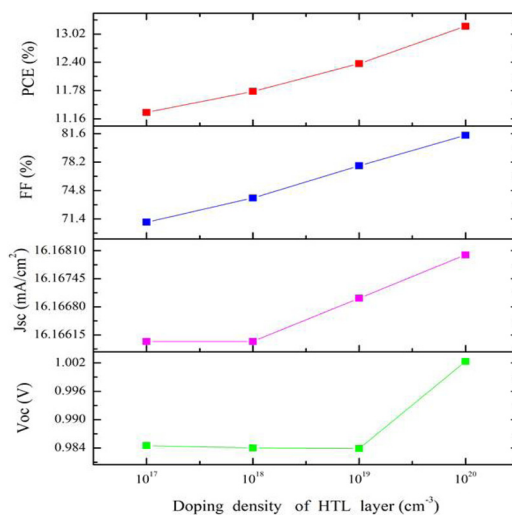**Fig. 7.** Effect of thickness of HTL layer on output parameters.

Fig. 8. Effect of doping density of HTL layer on output parameters.

parameters of solar cell, the reason being the illumination of the device from the front contact for the simulated conventional solar cell structure. The photogenerated charge carriers have higher density in HTL than in ETL and the defect density at HTL/Active interface has a strong influence on the output device performance and also is in agreement with the fact that lower defect density leads to better output.

3.4. Influence of HTL (CuI) properties

Hole transporting layer has a crucial impact on the output of OSC. Suitable selection of HTL provides better charge transport and charge collection at respective electrodes. We have studied the effect of input parameters of HTL layer such as thickness, doping concentration, electron affinity and mobility on the solar cell output.

The thickness of HTL layer has been varied from 30 nm to 50 nm and the effect on output parameters is shown in Fig. 7. The variation of thickness of the transport layer has negligible influence on the device output providing a consistent output for the entire range showing majority of the charge separation takes place in the active layer itself.

The effect of doping density of the hole transport layer on output parameters is shown in Fig. 8. As it appears, increasing the doping concentration of HTL results in improving the device output. This can be explained on the basis of increased conductivity of the cell leading to a reduced series resistance upon increasing the doping density. The reduction in series resistance is also visible in
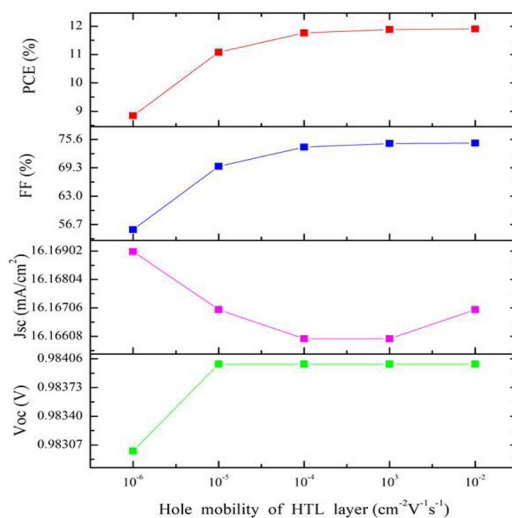
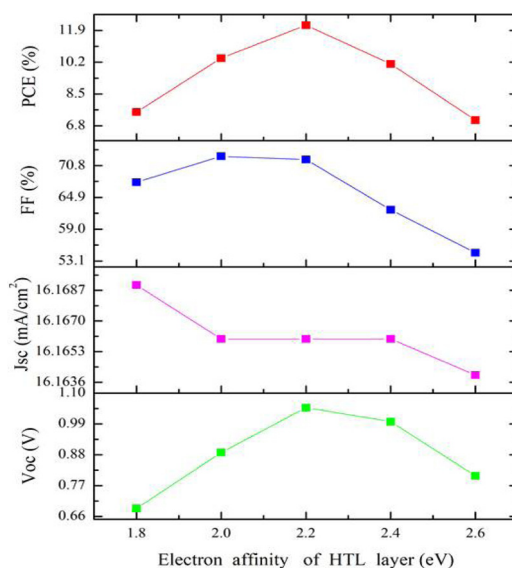**Fig. 9.** Effect of hole mobility of HTL layer on output parameters.

Fig. 10. Effect of electron affinity of HTL layer on output parameters.

the significant improvement in the fill factor of the solar cell upon increasing the doping concentration.

The effect of mobility of the hole transport layer is shown in Fig. 9. The hole mobility of HTL layer is being increased from $10^{-6}\,cm^2/Vs$ to $10^{-2}\,cm^2/Vs$ and effect is studied. As it appears, the output confirms the increase in conductivity of the material due to mobility effect.

The electron affinity of HTL is varied in the range 1.8–2.6 eV and the effect on output performance is shown in Fig. 10. PCE of 12.18% is achieved for optimum value at 2.2 eV. The optimum electron affinity reduce the bandgap effect providing better energy alignment and contributes to improved charge transport between the active layer and transport layers of non-fullerene organic solar cell [43].

3.5. Influence of ETL properties

The effect of ETL layer on the organic solar cell output is studied by varying its properties. The thickness of ETL layer is varied from 2 nm to 10 nm and the effect on the output parameters is shown in Fig. 11. The variation has little impact on output parameter similar to the case of HTL thickness.

The mobility of ETL layer is varied in the range from 10^{-6} to $10^{-2}\ {}^{cm^2}/Vs$ and the effect on output is shown in Fig. 12. The mobility influences the material conductivity and gives improved output.

The influence of doping density of ETL on the output parameters is shown in Fig. 13. The electron affinity is varied in the range
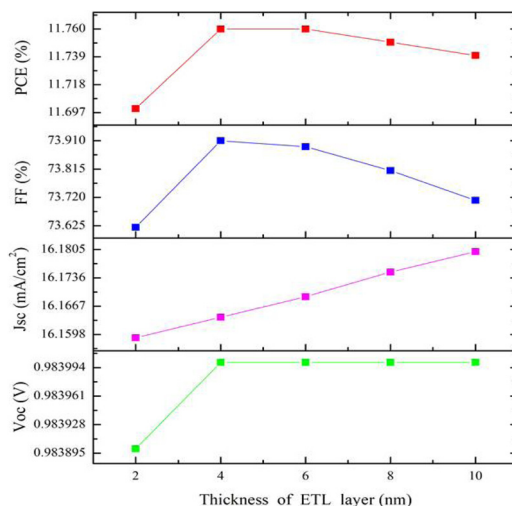
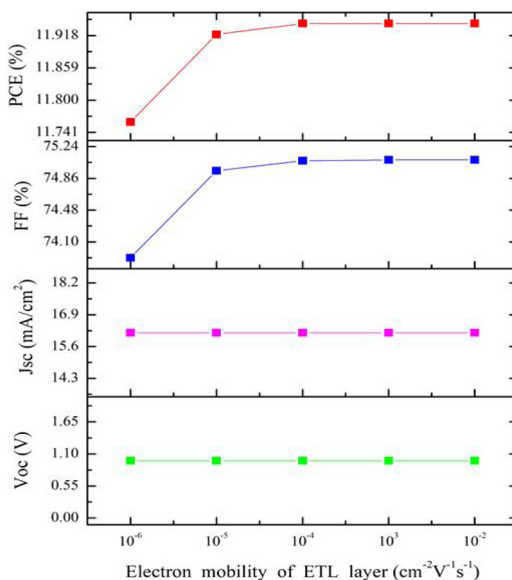**Fig. 11.** Effect of thickness of ETL layer on output parameters.

Fig. 12. Effect of electron mobility of ETL layer on output parameters.

from 3.9 eV to 4.3 eV and an improved efficiency of 11.87% is achieved at optimized value of 4.1 eV. The effect is shown in Fig. 14.

The optimized device parameters are summarized in Table 3. Simulating with optimized parameters, we obtained promising results, Voc of 0.9773 V, Jsc of 20.1525 mA/cm^2, FF of 79.59% and PCE of 15.68%. We compared the optimized results with the initial simulations in Table 4. Optimisation show that output of non-fullerene organic solar cell can be further enhanced with the use of inorganic CuI as the HTL.

4. Conclusion

The proposed structure of NFA-OSC with CuI as the HTL is simulated using SCAPS 1-D. We studied the effect of technological parameters on the output performance of the solar cell. The results have exhibited that the cell performance is improved upon increasing the thickness upto 200 nm and a lower defect density is crucial for better output performance. The defect density at HTL/Active interface has an impact on the output while that of Active/ETL interface is insignificant because of higher carrier density at the former. The transport layer characteristics are optimised in the simulation to improve efficiency. The cell performance with the optimised numerical parameters are Voc = 0.9773 V, Jsc = 20.1525 mA/cm^2, FF = 79.59% and PCE = 15.68%. The optimised result is encouraging for the use of CuI as an alternative to PEDOT:PSS, which is highly degrading and acidic for solar cell. We have successfully designed a NFA-OSC with inorganic CuI HTL with excellent efficiency upon optimization and the simulated results
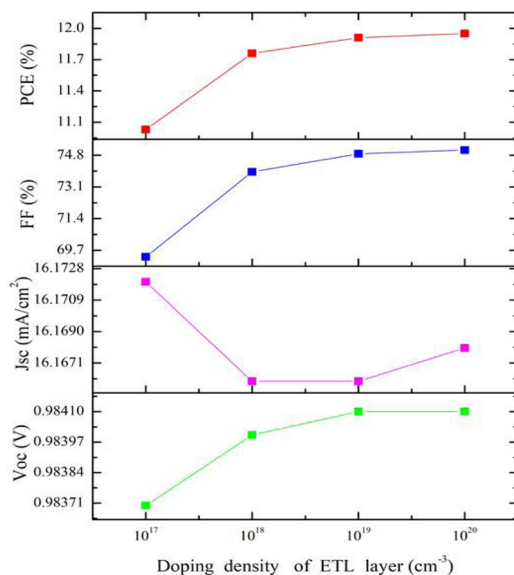
Fig. 13. Effect of doping density of ETL layer on output parameters.
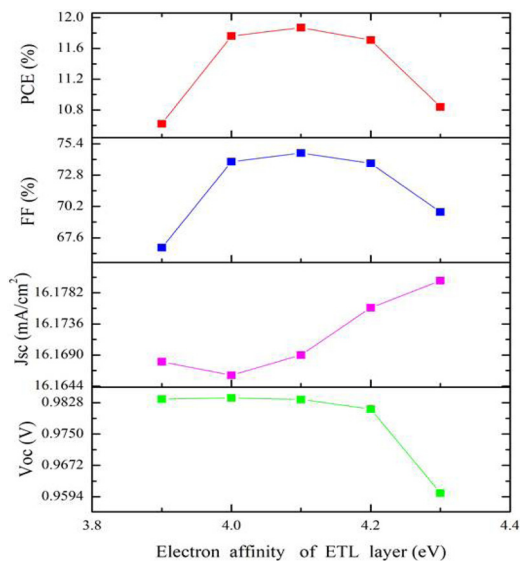
Fig. 14. Effect of electron affinity of ETL layer on output parameters.

Table 3
Optimized numerical parameters.

Parameters	ETL	Absorber	HTL
Doping density (cm^{-3})	10^{20}	–	10^{20}
Electron affinity (eV)	4.1	–	2.2
Thickness (nm)	–	200	-
Hole mobility ($cm^2V^{-1}s^{-1}$)	–	–	10^{-2}

promises to elevate the device performance of OSC in the near future.

Conflicts of interest

The authors declare no conflicts of interest.

Table 4

Device performance with optimized parameters.

Parameters	Thickness	χ	μ_p	Final
Voc (V)	0.9853	0.9836	0.984	0.9773
Jsc (mA/cm^2)	20.153	16.169	16.166	20.1525
FF (%)	68.39	74.63	74.69	79.59
PCE (%)	13.58	11.87	11.88	15.68

Acknowledgement

References

[1] K.M. Coakley, M.D. McGehee, Conjugated polymer photovoltaic cells, Chem. Mater. 16 (23) (2004) 4533–4542.

[2] B.A. Gregg, M.C. Hanna, Comparing organic to inorganic photovoltaic cells: theory, experiment, and simulation, J. Appl. Phys. 93 (6) (2003) 3605–3614.

[3] M.A. Green, K. Emery, Y. Hishikawa, W. Warta, E.D. Dunlop, Solar cell efficiency tables (version 45), Progress Photovolt.: Res. Appl. 23 (1) (2015) 1–9.

[4] M.C. Scharber, N.S. Sariciftci, Efficiency of bulk-heterojunction organic solar cells, Prog. Polym. Sci. 38 (12) (2013) 1929–1940.

[5] N. Gasparini, A. Wadsworth, M. Moser, D. Baran, I. McCulloch, C.J. Brabec, The physics of small molecule acceptors for efficient and stable bulk heterojunction solar cells, Adv. Energy Mater. 8 (12) (2018) 1703298.

[6] Q. An, W. Gao, F. Zhang, J. Wang, M. Zhang, K. Wu, X. Ma, Z. Hu, C. Jiao, C. Yang, Energy level modulation of non-fullerene acceptors enables efficient organic solar cells with small energy loss, J. Mater. Chem. A 6 (6) (2018) 2468–2475.

[7] G. Zhang, J. Zhao, P.C. Chow, K. Jiang, J. Zhang, Z. Zhu, J. Zhang, F. Huang, H. Yan, Nonfullerene acceptor molecules for bulk heterojunction organic solar cells, Chem. Rev. 118 (7) (2018) 3447–3507.

[8] X. Zhan, A. Facchetti, S. Barlow, T. Marks, M.A. Ratner, M.R. Wasielewski, S.R. Marder, Adv. Mater. 23 (2011) 268–284.

[9] Y. Lin, X. Zhan, Non-fullerene acceptors for organic photovoltaics: an emerging horizon, Mater. Horiz. 1 (5) (2014) 470–488.

[10] F.E. Ala'a, J.-P. Sun, I.G. Hill, G.C. Welch, Recent advances of non-fullerene, small molecular acceptors for solution processed bulk heterojunction solar cells, J. Mater. Chem. A 2 (5) (2014) 1201–1213.

[11] C.B. Nielsen, S. Holliday, H.-Y. Chen, S.J. Cryer, I. McCulloch, Non-fullerene electron acceptors for use in organic solar cells, Acc. Chem. Res. 48 (11) (2015) 2803–2812.

[12] H.-F. Yao, J.-H. Hou, et al., Design and Application of Highly Efficient Polymers for Polymer Solar Cells, (2016).

[13] Z. Hu, L. Ying, F. Huang, Y. Cao, Towards a Bright Future: Polymer Solar Cells, (2017), pp. 571–582.

[14] J.S. Kim, J.H. Park, J.H. Lee, J. Jo, D.-Y. Kim, K. Cho, Control of the electrode work function and active layer morphology via surface modification of indium tin oxide for high efficiency organic photovoltaics, Appl. Phys. Lett. 91 (11) (2007) 112111.

[15] S.W. Heo, E.J. Lee, K.W. Seong, D.K. Moon, Enhanced stability in polymer solar cells by controlling the electrode work function via modification of indium tin oxide, Sol. Energy Mater. Sol. Cells 115 (2013) 123–128.

[16] M. Irwin, B. Buchholz, A. Hains, R. Chang, T.J. Marks, p-type semiconducting nickel oxide as an efficiency-enhancing anode interfacial layer in polymer bulk-heterojunction solar cells, Proc. Natl. Acad. Sci. USA 105 (2008) 2783–2787.

[17] E.L. Ratcliff, B. Zacher, N.R. Armstrong, Selective interlayers and contacts in organic photovoltaic cells, J. Phys. Chem. Lett. 2 (11) (2011) 1337–1350.

[18] F. Zhang, M. Johansson, M.R. Andersson, J.C. Hummelen, O. Inganäs, Polymer photovoltaic cells with conducting polymer anodes, Adv. Mater. 14 (9) (2002) 662–665.

[19] G. Li, V. Shrotriya, J. Huang, Y. Yao, T. Moriarty, K. Emery, Y. Yang, High-efficiency solution processable polymer photovoltaic cells by self-organization of polymer blends, Materials For Sustainable Energy: A Collection of Peer-Reviewed Research and Review Articles from Nature Publishing Group (2011) 80–84.

[20] K. Wong, H. Yip, Y. Luo, K. Wong, W. Lau, K. Low, H. Chow, Z. Gao, W. Yeung, C. Chang, Blocking reactions between indium-tin oxide and poly (3, 4-ethylene dioxythiophene): poly (styrene sulphonate) with a self-assembly monolayer, Appl. Phys. Lett. 80 (15) (2002) 2788–2790.

[21] M. Kemerink, S. Timpanaro, M. De Kok, E. Meulenkamp, F. Touwslager, Three-dimensional inhomogeneities in pedot: pss films, J. Phys. Chem. B 108 (49) (2004) 18820–18825.

[22] H. Yan, P. Lee, N.R. Armstrong, A. Graham, G.A. Evmenenko, P. Dutta, T.J. Marks, High-performance hole-transport layers for polymer light-emitting diodes. Implementation of organosiloxane cross-linking chemistry in polymeric electroluminescent devices, J. Am. Chem. Soc. 127 (9) (2005) 3172–3183.

[23] Y.-H. Kim, S.-H. Lee, J. Noh, S.-H. Han, Performance and stability of electroluminescent device with self-assembled layers of poly (3, 4-ethylenedioxythiophene)-poly (styrenesulfonate) and polyelectrolytes, Thin Solid Films 510 (1–2) (2006) 305–310.

[24] P.A. Levermore, L. Chen, X. Wang, R. Das, D.D. Bradley, Fabrication of highly conductive poly (3,4-ethylenedioxythiophene) films by vapor phase poly-merization and their application in efficient organic light-emitting diodes, Adv. Mater. 19 (17) (2007) 2379–2385.

[25] X. Wang, T. Ishwara, W. Gong, M. Campoy-Quiles, J. Nelson, D.D. Bradley, High-performance metal-free solar cells using stamp transfer printed vapor phase polymerized poly (3,4-ethylenedioxythiophene) top anodes, Adv. Funct. Mater. 22 (7) (2012) 1454–1460.

[26] S.-S. Li, K.-H. Tu, C.-C. Lin, C.-W. Chen, M. Chhowalla, Solution-processable graphene oxide as an efficient hole transport layer in polymer solar cells, ACS Nano 4 (6) (2010) 3169–3174.

[27] J. Wei, Y. Jia, Q. Shu, Z. Gu, K. Wang, D. Zhuang, G. Zhang, Z. Wang, J. Luo, A. Cao, et al., Double-walled carbon nanotube solar cells, Nano Lett. 7 (8) (2007) 2317–2321.

[28] Y.-K. Han, M.-Y. Chang, K.-S. Ho, T.-H. Hsieh, J.-L. Tsai, P.-C. Huang, Electrochemically deposited nano polyaniline films as hole transporting layers in organic solar cells, Sol. Energy Mater. Sol. Cells 128 (2014) 198–203.

[29] V. Shrotriya, G. Li, Y. Yao, C.-W. Chu, Y. Yang, Transition metal oxides as the buffer layer for polymer photovoltaic cells, Appl. Phys. Lett. 88 (7) (2006) 73508.

[30] N. Yaacobi-Gross, N.D. Treat, P. Pattanasattayavong, H. Faber, A.K. Perumal, N. Stingelin, D.D. Bradley, P.N. Stavrinou, M. Heeney, T.D. Anthopoulos, High-efficiency organic photovoltaic cells based on the solution-processable hole transporting interlayer copper thiocyanate (cuscn) as a replacement for PEDOT:PSS, Adv. Energy Mater. 5 (3) (2015) 1401529.

[31] M. Grundmann, F.-L. Schein, M. Lorenz, T. Böntgen, J. Lenzner, H. von Wenckstern, Cuprous iodide-ap-type transparent semiconductor: history and novel applications, Phys. Status Solidi (a) 210 (9) (2013) 1671–1703.

[32] P. Stakhira, V. Cherpak, D. Volynyuk, F. Ivastchyshyn, Z. Hotra, V. Tataryn, G. Luka, Characteristics of organic light emitting diodes with copper iodide as injection layer, Thin Solid Films 518 (23) (2010) 7016–7018.

[33] S. Shao, J. Liu, J. Zhang, B. Zhang, Z. Xie, Y. Geng, L. Wang, Interface-induced crystalline ordering and favorable morphology for efficient annealing-free poly (3-

hexylthiophene): fullerene derivative solar cells, ACS Appl. Mater. Interfaces 4 (10) (2012) 5704–5710.

[34] W. Sun, H. Peng, Y. Li, W. Yan, Z. Liu, Z. Bian, C. Huang, Solution-processed copper iodide as an inexpensive and effective anode buffer layer for polymer solar cells, J. Phys. Chem. C 118 (30) (2014) 16806–16812.

[35] P. Cheng, G. Li, X. Zhan, Y. Yang, Next-generation organic photovoltaics based on non-fullerene acceptors, Nat. Photonics 12 (3) (2018) 131.

[36] X. Liu, B. Xie, C. Duan, Z. Wang, B. Fan, K. Zhang, B. Lin, F.J. Colberts, W. Ma, R.A. Janssen, et al., A high dielectric constant non-fullerene acceptor for efficient bulk-heterojunction organic solar cells, J. Mater. Chem. A 6 (2) (2018) 395–403.

[37] Z. Fei, F.D. Eisner, X. Jiao, M. Azzouzi, J.A. Röhr, Y. Han, M. Shahid, A.S. Chesman, C.D. Easton, C.R. McNeill, et al., An alkylated indacenodithieno [3,2-b] thiophene-based nonfullerene acceptor with high crystallinity exhibiting single junction solar cell efficiencies greater than 13% with low voltage losses, Adv. Mater. 30 (8) (2018) 1705209.

[38] X. Zhang, X. Zuo, S. Xie, J. Yuan, H. Zhou, Y. Zhang, Understanding charge transport and recombination losses in high performance polymer solar cells with non-fullerene acceptors, J. Mater. Chem. A 5 (33) (2017) 17230–17239.

[39] Y. Li, J.-D. Lin, X. Che, Y. Qu, F. Liu, L.-S. Liao, S.R. Forrest, High efficiency near-infrared and semitransparent non-fullerene acceptor organic photovoltaic cells, J. Am. Chem. Soc. 139 (47) (2017) 17114–17119.

[40] W. Zhao, D. Qian, S. Zhang, S. Li, O. Inganäs, F. Gao, J. Hou, Thermal stability, Adv. Mater. 28 (23) (2016) 4734–4739.

[41] O.M. Awartani, B. Gautam, W. Zhao, R. Younts, J. Hou, K. Gundogdu, H. Ade, Polymer non-fullerene solar cells of vastly different efficiencies for minor side-chain modification: impact of charge transfer, carrier lifetime, morphology and mobility, J. Mater. Chem. A 6 (26) (2018) 12484–12492.

[42] K.S. Nithya, S.K. Sudheer, Numerical modelling of non-fullerene organic solar cell with high dielectric constant itic-oe acceptor, J. Phys. Commun. (2020), https://doi.org/10.1088/2399-6528/ab772a.

[43] W. Abdelaziz, A. Shaker, M. Abouelatta, A. Zekry, Possible efficiency boosting of non-fullerene acceptor solar cell using device simulation, Opt. Mater. 91 (2019) 239–245.

[44] J. Löckinger, S. Nishiwaki, T.P. Weiss, B. Bissig, Y.E. Romanyuk, S. Buecheler, A.N. Tiwari, Tio2 as intermediate buffer layer in cu (in, ga) se2 solar cells, Sol. Energy Mater. Sol. Cells 174 (2018) 397–404.

[45] G.K. Gupta, A. Dixit, Theoretical studies of single and tandem Cu2ZnSn (s/se) 4 junction solar cells for enhanced efficiency, Opt. Mater. 82 (2018) 11–20.

[46] H.-J. Du, W.-C. Wang, J.-Z. Zhu, Device simulation of lead-free ch3nh3sni3 perovskite solar cells with high efficiency, Chin. Phys. B 25 (10) (2016) 108802.

[47] M.M. Salah, K.M. Hassan, M. Abouelatta, A. Shaker, A comparative study of different etms in perovskite solar cell with inorganic copper iodide as htm, Optik 178 (2019) 958–963.

[48] J. Kephart, J. McCamy, Z. Ma, A. Ganjoo, F. Alamgir, W. Sampath, Band alignment of front contact layers for high-efficiency cdte solar cells, Sol. Energy Mater. Sol. Cells 157 (2016) 266–275.

[49] B.S. Sengar, V. Garg, A. Kumar, V. Awasthi, S. Kumar, V.V. Atuchin, S. Mukherjee, Band alignment of cd-free (zn, mg) o layer with cu2znsn (s, se) 4 and its effect on the photovoltaic properties, Opt. Mater. 84 (2018) 748–756.

[50] A. Bauer, S. Sharbati, M. Powalla, Systematic survey of suitable buffer and high resistive window layer materials in cuin1-xgaxse2 solar cells by numerical simulations, Sol. Energy Mater. Sol. Cells 165 (2017) 119–127.

[51] S.Z. Haider, H. Anwar, M. Wang, A comprehensive device modelling of perovskite solar cell with inorganic copper iodide as hole transport material, Semicond. Sci. Technol. 33 (3) (2018) 35001.

[52] B.N. Ezealigo, A.C. Nwanya, A. Simo, R.U. Osuji, R. Bucher, M. Maaza, F.I. Ezema, Optical and electrochemical capacitive properties of copper (i) iodide thin film deposited by silar method, Arab. J. Chem. 12 (8) (2019) 5380–5391.

[53] J.H. Seo, T.-Q. Nguyen, Electronic properties of conjugated polyelectrolyte thin films, J. Am. Chem. Soc. 130 (31) (2008) 10042–10043.

[54] J. Liu, Y. Zhang, C. Liu, M. Peng, A. Yu, J. Kou, W. Liu, J. Zhai, J. Liu, Piezo-phototronic effect enhanced uv photodetector based on cui/zno double-shell grown on flexible copper microwire, Nanoscale Res. Lett. 11 (1) (2016) 281.

[55] O. Madelung, Iii-v compounds, Semiconductors: Data Handbook, Springer, 2004, pp. 71–172.

[56] Z. El Jouad, M. Morsli, G. Louarn, L. Cattin, M. Addou, J.C. Bernède, Improving the efficiency of subphthalocyanine based planar organic solar cells through the use of moo3/cui double anode buffer layer, Sol. Energy Mater. Sol. Cells 141 (2015) 429–435.

[57] M.I. Hossain, F.H. Alharbi, N. Tabet, Copper oxide as inorganic hole transport material for lead halide perovskite based solar cells, Sol. Energy 120 (2015) 370–380.

[58] B.M. Omer, A. Khogali, A. Pivrikas, Amps-1d modeling of p3ht/pcbm bulk-heterojunction solar cell, 2011 37th IEEE Photovoltaic Specialists Conference (2011) 000734–000743.

[59] M. Burgelman, P. Nollet, S. Degrave, Modelling polycrystalline semiconductor solar cells, Thin Solid Films 361 (2000) 527–532.

[60] Z. Zekry, G. Eldallal, Effect of ms contact on the electrical behaviour of solar cells, Solid-State Electron. 31 (1) (1988) 91–97.

[61] D. Yeboah, J. Singh, Dependence of exciton diffusion length and diffusion coefficient on photophysical parameters in bulk heterojunction organic solar cells, J. Electron. Mater. 46 (11) (2017) 6451–6460.